Climate Dynamics (2003) 20: 435–445
DOI 10.1007/s00382-002-0288-y

D.A. Stone · A.J. Weaver

Factors contributing to diurnal temperature range trends in twentieth and twenty-first century simulations of the CCCma coupled model

Received: 24 January 2002 / Accepted: 3 September 2002 / Published online: 14 November 2002

Abstract Trends in the diurnal temperature range (DTR) are examined in the late twentieth and the twenty-first centuries in a coupled climate model representing the atmosphere, ocean, sea ice, and land surface systems. Consistent with past studies, the DTR decreases during this time. These decreases are concentrated in middle latitudes, with much smaller changes occurring in the low latitudes. Strong seasonal characteristics to this pattern exist, although these are different in either hemisphere. In the model integrations, variations in the DTR are much more sensitive to changes in feedbacks than in direct forcings. The DTR is found to be insensitive to the scattering of sunlight by sulfate aerosols and the increased mean temperature. Instead, variations in the DTR arise mostly from changes in clouds and in soil moisture. Consequently, the decreasing trends stem from increases in the reflection of solar radiation by clouds moderated by decreases in soil moisture, mostly through its effect on the ground heat capacity. Both factors contribute about equally to the DTR trend. The exception to this relation occurs in the middle latitudes during winter, when snow cover reduces the influence of changes in solar radiation and soil moisture. Decreases during this season are a consequence of the artificial tendency in the model for the DTR to be very small when the mean temperature is near the freezing point. While the accuracy of these conclusions depends upon the model's ability to represent the relevant processes, the results highlight the importance of clouds and land surface processes to the DTR and its long-term change. The importance of soil moisture found here implies that changes in the physiological response of vegetation and in land use could have important effects on the DTR.

D.A. Stone (✉) · A.J. Weaver
School of Earth and Ocean Sciences, University of Victoria,
P.O. Box 3055, Victoria BC V8W 3P6, Canada
E-mail: stone@ocean.seos.uvic.ca

1 Introduction

The observed global mean trend towards warmer temperatures over land has been characterised by a large increase in the minimum daily temperatures (T_{min}) (Karl et al. 1993; Easterling et al. 1997; New et al. 2000; Jin and Dickinson 2002). Maximum daily temperatures (T_{max}) have increased at a much smaller rate, resulting in a decreasing trend in the diurnal temperature range (DTR), the magnitude of which is comparable to the mean warming itself. As an identifiable characteristic of recent climate change, this trend is important in diagnosing the forcing responsible for the change, and in particular the anthropogenic component. However, the cause of the DTR trend is still poorly understood, as is its relation to anthropogenic forcing.

Variations in cloud cover are strongly correlated with those in the DTR (Dai et al. 1997, 1999; New et al. 2000). The higher albedo of clouds decreases the downward solar radiation during the day, and thereby reduces T_{max}. Indeed, observational studies link the decreasing DTR to coincident increases in precipitating clouds (Karl et al. 1993; Dai et al. 1997, 1999). These low base clouds are particularly effective in reflecting sunlight, and changes in their frequency of occurrence would be expected to have the strongest impact on the DTR. Clouds also produce more downward long-wave radiation, so increasing nighttime cloud cover would increase T_{min} and thereby decrease the DTR. However, the tendency of the diurnal cycle of cloud cover over global land areas during recent years is currently unknown.

Soil moisture is also expected to influence the DTR, through control of evaporative cooling, the ground albedo, and the ground heat capacity. This effect tends to be most influential in the occurrence of extreme hot days (Durre et al. 2000). Dai et al. (1999) find that soil moisture is related to the DTR, albeit secondary to changes in cloud cover. This raises the possibility that the observed decreases in the DTR may be due in part to

physiological responses of vegetation to climate change or to changes in land use, although it appears that this latter factor is unable to account fully for the observed changes (Easterling et al. 1997; Gallo et al. 1999).

Atmospheric and coupled general circulations models (GCMs) predict a decrease in the DTR under enhanced greenhouse forcing (Cao et al. 1992; Mitchell et al. 1995; Colman et al. 1995; Reader and Boer 1998; Dai et al. 2001), but the magnitude of this change is considerably smaller than observed (Stone and Weaver 2002). In agreement with energy balance models (Cao et al. 1992; Stenchikov and Robock 1995), the addition of the scattering effect of sulfate aerosols produces little difference in the DTR change (Mitchell et al. 1995; Reader and Boer 1998; Stone and Weaver 2002). Stenchikov and Robock (1995) note that in an energy balance model the DTR is quite sensitive not only to mean changes in cloud coverage, but also to the nature of the diurnal cycle of the coverage. Indeed, Dai et al. (2001) find in a coupled GCM integration that the reduction in the DTR is associated with changes in cloud coverage, as well as with changes in soil moisture. However, Collatz et al. (2000) note that the physiological response of vegetation, which is not represented in these models, could also be a rather important influence.

To better understand its relation to current climate change this work examines the nature and cause of trends in the DTR in integrations of a coupled GCM. The model and the integrations are described briefly in Sect. 2. Sec. 3 consists of a detailed examination of the DTR trends produced in the model integrations. In Sect. 4 a simple analytic model is used to diagnose possible causes for the trends, while in Sect. 5 statistical models are used to isolate these causes further. The cause of the DTR trends in the middle latitude winter is not evident from the analyses in these two sections, and thus is examined more closely in Sect. 6. The results are discussed in Sect. 7.

2 Model

The model used in this investigation is the first generation coupled GCM of the Canadian Centre for Climate Modelling and Analysis (CCCma), known as CGCM1 (Flato et al. 2000). It includes comprehensive representations of the atmosphere, ocean, sea ice, and land surface. While Reader and Boer (1998) and Stone and Weaver (2002) also examine DTR changes in integrations of this model, here we conduct a more thorough analysis of the spatial characteristics of this global trend, and examine its relation to other climate variables.

The atmospheric component of CGCM1 is a spectral model with triangular truncation at wavenumber 32 (McFarlane et al. 1992). This yields a surface grid resolution of about 3.75°. A hybrid topographic-pressure vertical coordinate system is employed resulting in 10 unequally spaced levels. A land surface scheme underlies the atmospheric component, and uses a single soil layer with spatially varying moisture field capacity and soil properties.

Screen level temperature is estimated from temperatures at the lowest level (200 m) and the surface using a gradient profile relationship. To resolve the diurnal cycle adequately, full solar radiation calculations are performed every 3 h, with the radiation at intervening time steps (20 min) extrapolated from the full calculation based upon the solar zenith angle. Full calculations of the terrestrial radiation are performed every 6 h, with partial calculations at intervening time steps which re-evaluate the fluxes and heating rates using emissivities computed during the previous full calculation.

The ocean component is a grid point model with double the horizontal resolution of the atmosphere (1.875°) and 29 unequally spaced vertical levels. A simple one-dimensional thermodynamic sea-ice model is used. In order to prevent drift of the model integration toward less realistic states, heat and fresh water flux adjustments are used between the atmosphere and ocean (Flato et al. 2000).

We use an ensemble of three global warming integrations from CGCM1 covering the 1900–2100 interval (CGCM1 GHG + A1,2,3), although we concentrate on the output of CGCM1 GHG + A1. In these integrations the model is forced with the observed atmospheric concentrations of greenhouse gases and sulfate aerosols until present, and with those projected for the future according to a modified version of the IPCC 1992a scenario (Boer et al. 2000a, b). The direct scattering of sunlight by sulfate aerosols is included by altering the surface albedo (Reader and Boer 1998); the indirect effect of aerosols, whereby they alter the lifetime and optical properties of clouds, is not included. The three integrations are identical except for the initial atmospheric conditions, and thus represent independent possible realisations of recent and future climate. A similar integration which lacks the scattering effect of sulfate aerosols (CGCM1 GHG) is also examined in order to determine the importance of the aerosols for the DTR trend. Finally, a 201 year control integration (CGCM1 CTRL), which uses constant pre-industrial forcings, is used as a reference. These model integrations are listed and compared in Table 1.

We also examine an ensemble of three integrations of a more recent version of the CCCma coupled model, known as CGCM2 (CGCM2 GHG + A1,2,3). This model uses different representations of ocean mixing and sea ice (Flato and Boer 2001). In particular, the Gent and McWilliams parametrisation associated with mesoscale eddies (Gent and McWilliams 1990) and a cavitating fluid representation of sea ice (Flato and Hibler 1992) are included. An important result of these modifications is a much larger warming of the surface at middle and high southern latitudes, producing a more meridionally symmetric warming pattern (Flato and Boer 2001). The details of the integration procedure are identical to the CGCM1 GHG + A integrations.

Since the climate does not change substantially until 1950, we examine the 1950–2100 interval here. The DTR over the ocean is quite small, and so trends in the DTR are negligible, if even detectable in the observations. Therefore, only land areas are included in the analysis. Areas poleward of the Arctic and Antarctic circles are also excluded since the DTR does not represent the daytime-nighttime cycle at these latitudes. CGCM1 lacks an ice-sheet model, resulting in a build-up of moisture over ice sheets. Since this complicates comparison of the DTR to other climate variables, the southern tip of Greenland is also excluded.

3 Trends

Stone and Weaver (2002) directly compare the DTR trends in CGCM1 integrations with those observed by

Table 1 A list of the model integrations used in this study

Model	Integration	Increasing greenhouse gas concentrations	Increasing aerosol concentrations
CGCM1	CTRL	No	No
CGCM1	GHG	Yes	No
CGCM1	GHG + A1	Yes	Yes
CGCM1	GHG + A2	Yes	Yes
CGCM1	GHG + A3	Yes	Yes
CGCM2	GHG + A1	Yes	Yes
CGCM2	GHG + A2	Yes	Yes
CGCM2	GHG + A3	Yes	Yes

Easterling et al. (1997) over the 1950–1993 period. While the integrations indicate a tendency toward decreasing DTR, these trends are smaller than observed by about two thirds. Here we more closely examine the spatial nature of the model trends over land areas, looking particularly at the 1950–2100 period. The annual mean time series of the DTR, T_{min}, and T_{max} in CGCM1 GHG + A1 over this interval are shown in Fig. 1. The data used cover all land areas (except for the polar restrictions). The DTR increase, which starts around 1970 and is rather linear thereafter, is much smaller than the trend in the mean temperature, and thus is not entirely consistent with the observed changes.

The mean annual trends in the DTR during the December–January (DJF) and June–August (JJA) seasons over the 1950–2100 period from CGCM1 GHG + A1 are displayed in Fig. 2. The spatial pattern is very similar in the other global warming integrations. It does not, however, resemble the observed spatial pattern of Easterling et al. (1997), though Stone and Weaver (2002) note that the observed pattern may not be robust over the 44 years of observations. The DTR rather uniformly decreases in the middle northern latitudes, but in other areas there is a more regional mix of positive and negative trends. Most of the differences occur on regional scales, with the pattern being rather smooth at the model resolution.

To understand this pattern of trends better, we examine them separately for each season and for four zonal bands, covering the 66°S–33°S, 33°S–0°, 0°–33°N, and 33°N–66°N intervals. These divisions correspond approximately to changes in the seasonal behaviour of the DTR and in its relation to other climate variables. In particular, the relative importance of T_{min} and T_{max} in determining the DTR changes near 33° during the winter (and near 66° during the summer) in both hemispheres. Trends over these regions in the CGCM1 GHG + A integrations during the 1950–2100 period are displayed schematically in Fig. 3.

Some of the largest decreases occur in the middle northern latitudes during DJF and March–May (MAM), while changes are minimal in the other two seasons. The mean temperature rises faster in DJF and MAM, and so the DTR decreases result from particularly large increases in $T_{\min}$. Decreases in the DTR about half as large also occur in the low northern latitudes in DJF and MAM, as well as during September–November (SON). The mean warming is also very similar in these seasons. The exception of JJA results mainly from a slower warming of T_{min}.

DTR changes are small in all seasons in the low southern latitudes, with mean temperature increases also rather similar in each season. However, the middle southern latitude DTR trends are of comparable

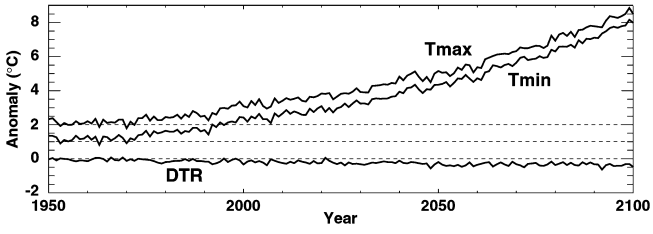

Fig. 1 Global mean variations in T_{max}, T_{min}, and the DTR in CGCM1 GHG + A1. Values are averaged over non-polar land areas. Anomalies from the CGCM1 CTRL mean are shown, with T_{max}, and T_{min} values shifted up by 2 °C and 1 °C respectively

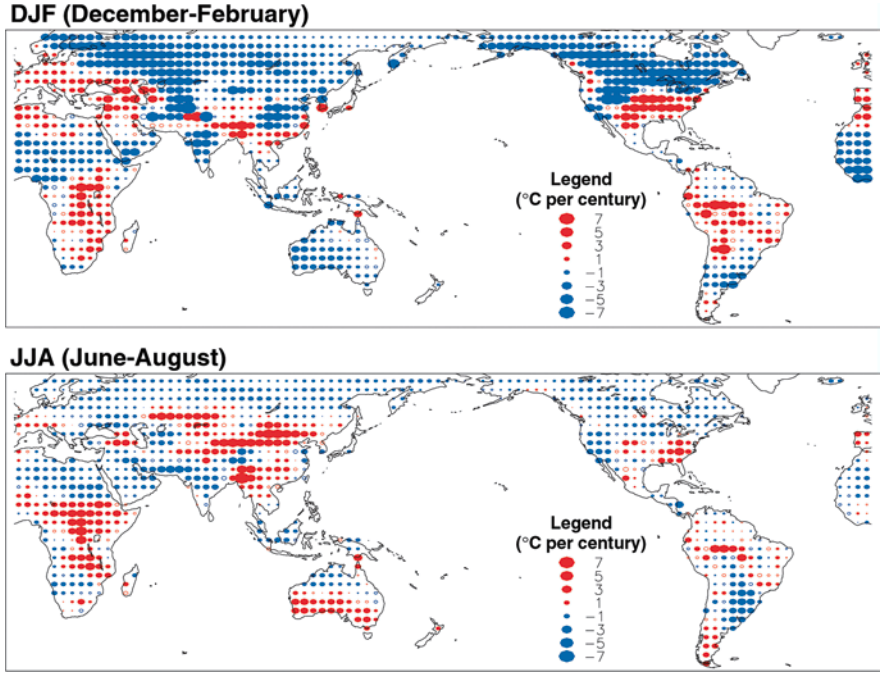

Fig. 2 1950–2100 mean trends in the DTR in CGCM1 GHG + A1 during the DJF and JJA seasons. Values are shown over non-polar land areas only. *Solid bullets* denote trends statistically significant at the 5% level, assuming a white noise process

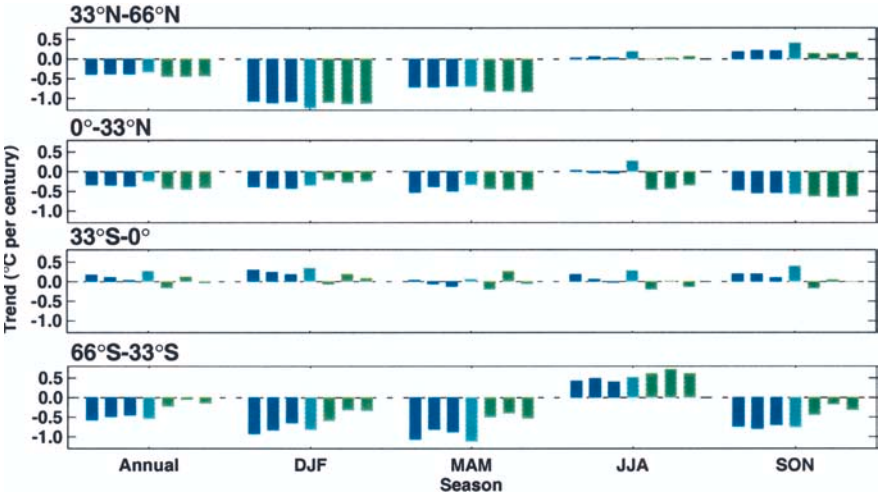

Fig. 3 Annual and seasonal mean trends in the DTR during the 1950–2100 interval over four zonal bands. Values are calculated for land areas only. For each season the *three blue bars* represent trends in the CGCM1 GHG + A integrations, while the *cyan bar* represents the trend in CGCM1 GHG. The *green bars* represent trends in three integrations of the CGCM2 model forced with changes in greenhouse gases and sulfate aerosols similar to those imposed in the CGCM1 GHG + A integrations

magnitude to those in the middle northern latitudes, while the mean warming is much smaller than in the other regions. This region experiences large decreases in the DTR in SON, DJF, and MAM. The anomalous increase in the DTR during JJA is due to a smaller warming of T_{min}. The similarity to the calendar season pattern in northern middle latitudes is puzzling considering the phase difference in the seasons between both hemispheres. Of course, while the trends appear consistent between integrations, it should be remembered that the southern middle latitudes contain very little land. Furthermore, this land is close to the low latitudes, and so the climatology here may not properly represent that over middle latitude land masses.

Stone and Weaver (2002) note that the CGCM2 GHG + A integrations predict more negative DTR trends in the Southern Hemisphere than do the GHG + A integrations of CGCM1, in better agreement with the observations, whereas the two models differ little in the Northern Hemisphere trends. The important difference between the two models is the use of the Gent and McWilliams mixing parametrisation in CGCM2, which results in a larger warming in the Southern Hemisphere. The hemispheric characteristics of the DTR trends from the two models also hold over the longer 1950–2100 period and full global landmass (Fig. 3). Practically indentical trends occur over the Northern Hemisphere in the integrations of both models during most seasons. In the lower southern latitudes, however, the trends tend to be more negative in the CGCM2 GHG + A integrations, although in both models the change is small. Over the middle southern latitudes, on the other hand, the trends are substantially more positive. However, since most of Southern Hemisphere landmass is in the lower latitudes, the hemispheric trends closely resemble those for this region. Stone and Weaver (2002) suggest that this difference between the model results in the Southern Hemisphere arises from increased land clouds produced by the warmer ocean. Indeed, the decrease in solar radiation at the surface is 40% larger over the Southern Hemisphere in the CGCM2 GHG + A integrations than in those of CGCM1, whereas little difference exists in the Northern Hemisphere. The importance of clouds for the DTR trends is examined further in the next two sections.

Trends in the DTR in CGCM1 GHG are also displayed in Fig. 3. The single difference between this and the CGCM1 GHG + A integrations is the absence of scattering due to sulfate aerosols. This results in a considerably larger mean warming. However, as noted previously (Mitchell et al. 1995; Reader and Boer 1998; Stone and Weaver 2002), exclusion of this forcing produces little change in the DTR trend. In some cases the omission results in very slightly more positive trends, but the general effect is minimal.

4 Physical analysis of factors influencing the DTR

The diurnal temperature range is influenced by several factors, many of which could change under global warming. To diagnose the relative importance of these factors we formulate a first order analytic calculation of the DTR. The intention here is simply to identify climate variables to which the DTR is directly most sensitive, and which therefore could induce a trend under global warming. Of course, this calculation will require many approximations, but the advantage lies in the simplicity of its physical interpretation. We stress that this calculation is intended for interpretive purposes only, and is not intended to exhaustively represent all of the processes operating during the diurnal cycle. More accurate, but less physically intuitive, statistical models will be used in the next section to support the conclusions from this analytic calculation.

The rate of change of the energy flux at the surface is given by

$$c_a \frac{\partial T}{\partial t} = S + L_{\downarrow} + L_{\uparrow} + H_l + H_s + G + U \quad . \tag{1}$$

Here c_a is the heat capacity of the air, T is the screen level temperature, t is time, S is the incoming solar

radiative flux, $L\downarrow$ and $L\uparrow$ are the incoming and outgoing terrestrial long-wave radiative fluxes, H_l and H_s are the latent and sensible heat fluxes, G is the flux into the ground, and U is the horizontal advective term.

We start by taking the diurnal cycle to be a step function, jumping instantaneously from nighttime to daytime values. A more accurate description would result in a much more complicated solution than the first order model desired here. Once again, we stress that this calculation is for interpretative purposes only, and thus such approximations are permitted. From Eq. (1), the change of surface temperature (ΔT) from night to day (Δt) is then

$$c_a \frac{\Delta T}{\Delta t} \sim S_d + L_{\downarrow_d} + L_{\uparrow_d} + H_{l_d} + H_{s_d} + G_d + U_d - S_d - L_{\downarrow_n} - L_{\uparrow_n} - H_{l_n} - H_{s_n} - G_n - U_n \quad (2)$$

where the d and n subscripts denote typical daytime and nighttime values.

The heat capacity of the air is defined as

$$c_a = \rho C_p h$$

where ρ is the density of the air (1.3 kg $\cdot$ m^{-3}), C_p is the specific heat (1.0×10^3 J $\cdot$ K^{-1}kg^{-1}), and h is the 2 m distance between the measurement level and the surface.

The daytime solar flux at the surface can be approximated as

$$S_d \sim S_0(1 - f_c\alpha_c)(1 - \alpha_g)$$

where S_0 is the average daytime solar radiative flux at the top of the atmosphere, α_c and α_g are the cloud and ground albedos, and f_c is the fraction of the sky covered by cloud. Since

$$S_c \sim S_0(1 - f_c\alpha_c) \quad (3)$$

is archived in the model, while α_c is not, we use S_c instead. S_n is obviously zero.

The incoming longwave flux possesses only a small diurnal cycle (e.g. Dai et al. 1999) which can be considered negligible for the present purposes ($L\downarrow_d \sim L\downarrow_n$). Meanwhile, under the step function assumption the outgoing long-wave radiation is given by $L\uparrow_d \sim \sigma T^4{}_{max}$ and $L\uparrow_n \sim -\sigma T^4{}_{min}$, where σ is the Stefan-Boltzmann constant. The emissivity is omitted here since it is prescribed as unity for all surfaces in CGCM1 (Norm McFarlane personal communication). Upon linearisation about some T_0 near T_{max} and T_{min}, this yields a difference of

$$L\uparrow_d - L\uparrow_d \sim -4\sigma T_0^3 \Delta T \ .$$

We combine the latent and sensible heat fluxes since they are forced by similar processes, exhibit similar diurnal cycles (Barry and Chorley 1992), and have identical effects on the screen temperature. We assume zero flux during the night, and a constant value during the day, yielding

$$H_d \equiv H_{l_d} + H_{s_d} \sim H_0$$

where H_0 is the average daytime heat flux.

The energy absorbed by the ground can be written as

$$G = -c_g \frac{\partial T_g}{\partial t}$$

where c_g is the effective heat capacity of the ground and T_g is its effective temperature. The magnitude of the diurnal temperature wave into the ground decreases as a function of depth, and so using just the heat capacity of soil would be inappropriate. This effect of vertical diffusion is absorbed into the value of c_g. For convenience, we approximate T_g by the air temperature. Since c_g depends upon the soil moisture, it can be described by

$$c_g \sim c_{g_0} + c_{g_1} w_g$$

where c_{g_0} is the effective heat capacity of dry soil and c_{g_1} is the rate of change of the effective heat capacity as a function of the soil moisture fraction w_g.

Finally, since advection should be uncoupled from the diurnal cycle at most locations we defined U_d and U_n to be equal, and thus they cancel over the diurnal cycle.

Substituting these approximations into Eq. (2), we find that

$$\Delta T \sim \frac{S_c(1 - \alpha_g) - H_0}{c_a + c_{g_0} + c_{g_1} w_g + 4\sigma T_0^3 \Delta t} \Delta t \ . \quad (4)$$

Annual global mean values of the parameters in Eq. (4) are listed in Table 2. The domain (global or zonal band) average obtained from CGCM1 CTRL is used for most parameters. Domain averages are used for c_{g_0} and c_{g_1} (Daniel Robitaille personal communication). Estimation of the DTR with these parameter values yields 15 K, which compares reasonably with the actual value of 11 K from CGCM1 CTRL, considering the many approximations.

The correlations between ΔT from Eq. (4) and the model DTR over the four zonal bands are listed in Table 3 for the DJF and JJA seasons. In each row of the table, the time series of each indicated variable is included in the calculation, with the other parameters being held constant. c_a is assumed constant in all cases since its

Table 2 Annual mean values for the parameters in Eq. (4) averaged over global land areas

Parameter	Name	Value
S_c	Mean daytime solar radiation	420 W $\cdot$ m^{-2}
α_g	Ground albedo	0.24
Δ_t	Time interval	3.2×10^4 s
c_a	Air heat capacity	2.6×10^3 J $\cdot$ K^{-1} $\cdot$ m^{-2}
c_{g_0}	Dry soil heat capacity	8.5×10^4 J $\cdot$ K^{-1} $\cdot$ m^{-2}
c_{g_1}	Wet soil heat capacity factor	7.9×10^4 J $\cdot$ K^{-1} $\cdot$ m^{-2}
w_g	Soil moisture fraction	0.45
H_0	Mean daytime heat fluxes	180 W $\cdot$ m^{-2}
σ	Stefan-Boltzmann constant	5.7×10^{-8} W $\cdot$ K^{-4} $\cdot$ m^{-2}
T_0	Mean surface temperature	290 K

mean and variance are an order of magnitude smaller than those of the other terms. For the results in Table 3, values were averaged over time and space before being input into Eq. (4). The correlations at each grid point for annual mean values are displayed in Fig. 4.

S_c and w_g are both individually highly correlated with the DTR in most cases. Little skill is added by the inclusion of the variability from the other factors. While the sensible and latent heat fluxes are each highly correlated with the DTR (not shown), their sum is mostly unrelated to it, consistent with the results of observational studies (Dai et al. 1999).

Exceptions to the high correlation between both S_c and w_g with the DTR occur during the winter seasons in the middle latitudes. During these seasons snow covers most of these areas, which reflects sunlight and thus reduces the diurnal amplitude of the solar radiative forcing. Also, snow insulates the air from the ground, damping the moderating effect of the soil moisture's heat capacity. It is not surprising that neither variable is strongly related to the DTR in these cases. Unfortunately, it is not clear from Table 3 what replaces these factors in controling the DTR; this will be examined more closely in Sect. 6.

The 1950–2100 trends in CGCM1 GHG + A1 predicted by Eq. (4) with the inclusion of the changes in the various variables are compared to the model DTR trends in Table 4. The DTR tendency is most sensitive to the changes in S_c, but the estimated trends are considerably more negative than the actual model DTR trends in most cases. Inclusion of the changes in the remaining variables does not result in any substantial improvement in accuracy, and in fact tends to make the estimates even more negative. The similarity between the estimated and model DTR trends is not as good as would be expected from the high correlations listed in Table 3. However, the pattern of estimated trends made using all inputs resembles the pattern of actual model trends but with a more negative average, suggesting a systematic bias in the formulation of Eq. (4). This same pattern exists in the estimates made with only S_c and w_g as inputs, further suggesting that the bias involves one of these variables. It appears that either the effect of S_c is being overestimated (since it tends to predict negative trends) or that the effect of w_g is being underestimated (since it tends to predict positive trends). We now turn to a statistical examination of the model output to resolve this question by showing that w_g is in fact being underestimated.

Table 3 Correlation between the model DTR from CGCM1 CTRL and estimates from Eq. (4). For each estimate, the time series from CGCM1 CTRL is used for the indicated variable(s); other variables are assumed constant at their mean value. Seasonal means of the variables were averaged over the zonal bands before input into the equation. Coefficients outside of the –0.1 to 0.1 interval are significant at the 5% level assuming white noise processes

Variable	66–33°S		33°S–0°		0°–33°N		33–66°N	
	DJF	JJA	DJF	JJA	DJF	JJA	DJF	JJA
S_c (solar radiation)	0.8	0.2	0.9	0.8	0.7	0.9	0.5	0.9
α_g (ground albedo)	–0.9	–0.2	–0.5	–0.6	–0.2	–0.4	–0.5	0.1
H_0 (heat fluxes)	0.2	0.1	0.0	0.7	0.4	0.1	0.2	–0.2
w_g (soil moisture)	0.9	0.7	0.8	0.8	0.6	0.8	0.2	0.8
T_0 (mean temperature)	–0.4	–0.7	–0.6	–0.5	0.0	–0.6	0.5	–0.6
S_c, α_g, H_0, w_g, T_0	1.0	0.4	1.0	0.9	0.8	1.0	0.1	0.8
S_c, w_g	0.9	0.5	0.9	0.9	0.8	0.9	0.5	0.9

5 Statistical analysis

Calculations with Eq. (4) indicate that the radiative effects of clouds and the heat capacity of soil moisture are the controling influences on the DTR. However, the analytic model is quite simple and makes many approximations. The effects of this are most evident in the estimated DTR trends, which are not entirely similar to the model changes. However, the analytic model was useful in providing a physical framework for this investigation. In this section we turn to linear regression models to confirm the importance of clouds and soil moisture to the DTR trends, and to resolve the question of the systematic bias found above. While these statistical models lack the physical insight of the analytic model of Eq. (4), they will likely yield more accurate results since their construction depends on the data themselves.

The regression models are constructed according to

$$\Delta T_{\mathrm{GHG+A1}} \sim \overline{DTR}_{\mathrm{CTRL}} + \frac{s_{DTR_{\mathrm{CTRL}}}}{s_{x_{\mathrm{CTRL}}}} r_{DTR,x_{\mathrm{CTRL}}} \times \left(x_{\mathrm{GHG+A1}} - \bar{x}_{\mathrm{CTRL}}\right) . \quad (5)$$

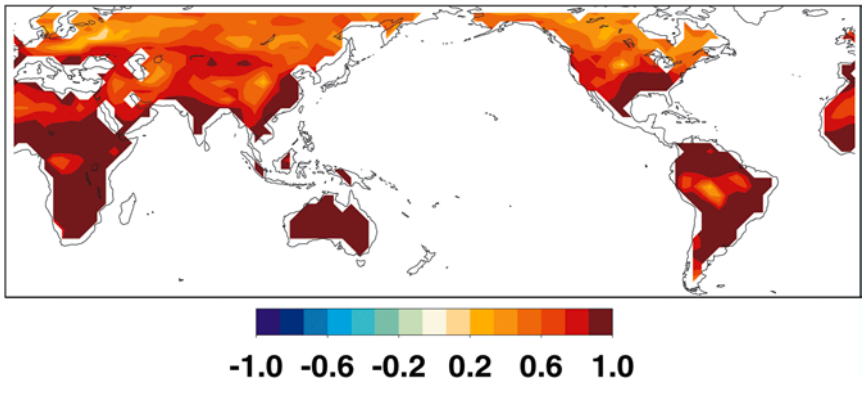

Fig. 4 Map of the correlation between the annual mean DTR in CGCM1 CTRL and estimates from Eq. (4). Annual mean values for S_c, α_g, H_0, w_g, and T_0 from CGCM1 CTRL were used in the calculation

Table 4 1950–2100 trends in the DTR in the CGCM1 GHG + A1 integration estimated from Eq. (4). For each estimate, the time series from GHG + A1 is used for the indicated variable(s); other variables are assumed constant at the mean values in CGCM1 CTRL. Trends are in °C per century

Variable	66–33°S		33°S–0°		0°–33°N		33–66°N	
	DJF	JJA	DJF	JJA	DJF	JJA	DJF	JJA
DTR	–0.9	0.4	0.3	0.2	–0.4	0.0	–1.1	0.0
S_c (solar radiation)	–1.7	–0.1	–0.7	–0.6	–1.2	–0.3	–0.5	–1.1
α_g (ground albedo)	–0.5	–0.2	–0.5	–0.5	–0.6	–0.7	1.0	0.1
H_0 (heat fluxes)	0.1	–0.4	0.5	0.2	0.2	0.0	–0.6	–0.5
w_g (soil moisture)	–0.3	–0.5	0.3	0.3	0.2	0.2	0.0	0.1
T_0 (mean temperature)	–0.4	–0.2	–0.3	–0.4	–0.5	–0.4	–0.4	–0.4
S_c, α_g, H_0, w_g, T_0	–2.6	–1.4	–0.7	–1.1	–1.8	–1.1	–0.5	–1.8
S_c, w_g	–2.0	–0.7	–0.4	–0.4	–1.1	0.0	–0.4	–1.0

Here ΔT is the estimated DTR, x is some other climate variable, s_{DTR} and s_x are the standard deviations of the DTR and of variable x, and r_{DTR_x} is the correlation coefficient between the DTR and x. The subscripts denote the integration from which the values are drawn, while the bar denotes the temporal average. Therefore, this statistical model is constructed using the correlation between variables in CGCM1 CTRL, but is then applied to the data from CGCM1 GHG + A1.

The correlation between the model DTR and the estimates from Eq. (5) using the listed input variables are given in Table 5 for the DJF and JJA seasons in CGCM1 GHG + A1 over the four zonal bands. The test uses CGCM1 GHG + A1 output since the model specifically finds the best fit to the CGMC1 CTRL output, and so this test is not affected by possible overfitting. However, since rather large trends occur and dominate the variance in many of the variables in CGCM1 GHG + A1, the second order least squares polynomial fit is removed from all time series before the calculation of the correlation. As required by the values in Table 3, estimates produced either by S_c or by w_g are highly correlated with the DTR at high frequencies, and use of both variables generally improves the estimate. The exceptions are of course, the winter seasons at middle latitudes.

The DTR trends expected in CGCM1 GHG + A1 according to these estimates are listed in Table 6. As expected, use of S_c produces similar trend estimates to those in Table 4 using the analytic model with S_c. However, the trends estimated with w_g are generally much larger than the corresponding values in Table 4, suggesting that the bias in Eq. (4) lies in an underestimation of the effect of soil moisture. Indeed, the combined use of the two predictands S_c and w_g produces estimates very similar to the model trends, with the not surprising exception of the winter seasons trends over the middle latitudes. The global annual mean 1950–2100 variations in the DTR estimate based on solar radiation and soil moisture are shown in Fig. 5. The strong similarity to the model DTR variations is consistent throughout the time period. The corresponding trends at each grid point are displayed in Fig. 6.

From Eq. (3), S_c is a function of both f_c and α_c. Since the latter is not archived from the CGCM1 integration we examine f_c to determine the cause of the changes in S_c. In fact, S_c and f_c are very highly correlated and are comparable in their relation to the DTR (Table 5). However, the estimated trends in the DTR in CGMC1 GHG + A1 differ systematically by about 1 °C/century (Table 6). The increased absorption of solar infrared radiation by more water vapour in a warmer atmosphere has been suggested as a partial forcing of the DTR trend (Stenchikov and Robock 1995), and would manifest here as a trend in S_0. However, the expected magnitude of this effect is too small to account for the discrepancy here. That leaves a trend in α_c or in the diurnal cycle of cloud cover as possible causes. The increase of precipitation over land in CGCM1 (Boer et al. 2000b) indicates taller and thicker clouds with larger water droplets, which suggests that an increase in α_c is plausible.

Soil moisture and solar radiation are strongly related at the seasonal time scales examined here. Soil moisture is determined by precipitation and evaporation, both of which are related to clouds and thus solar radiation. Conversely, clouds depend upon the availability of water vapour, which in turn depends on the soil moisture.

Table 5 Correlations between the model DTR and linear regression estimates. Values are calculated from the output of CGCM1 GHG + A1 after removal of the second order least squares polynomial fit, and span four zonal regions. Seasonal means of the variables were averaged over the zonal bands before input into the equation. $S_{c_{res}}$ ($w_{g_{res}}$) is the residual of S_c (w_g) after removal of the component correlated with w_g (S_c). See the text for a description of the regression estimation. Values outside of the –0.1 to 0.1 interval are significant at the 5% level assuming white noise processes

Variable	66–33°S		33°S– 0°		0°–33°N		33–66°N	
	DJF	JJA	DJF	JJA	DJF	JJA	DJF	JJA
S_c (solar radiation)	0.8	0.5	0.9	0.8	0.7	0.9	0.4	0.9
S_{cres} (S_c residual)	0.3	0.3	0.6	0.5	0.7	0.5	0.4	0.5
f_c (cloud fraction)	0.7	0.3	0.9	0.8	0.8	0.9	0.5	0.9
w_g (soil moisture)	0.8	0.7	0.8	0.8	0.5	0.8	0.2	0.8
$w_{g_{res}}$ (w_g residual)	0.6	0.7	0.4	0.5	0.3	0.3	0.2	0.3
S_c, w_g	0.9	0.7	1.0	0.9	0.8	0.9	0.4	0.9

Table 6 Trends in the DTR and estimates from linear regression models. Values are in °C/century, span four zonal regions, and are calculated from the output of CGCM1 GHG + A1. $S_{c_{res}}$, and $w_{g_{res}}$ are defined in Table 5. See the text for a description of the regression models

Variable	66–33°S		33°S–0°		0°–33°N		33–66°N	
	DJF	JJA	DJF	JJA	DJF	JJA	DJF	JJA
DTR	–0.9	0.4	0.3	0.2	–0.4	0.0	–1.1	0.0
S_c (solar radiation)	–1.0	0.0	–0.5	–0.6	–0.9	–0.2	–0.2	–0.7
$S_{c_{res}}$ (S_c residual)	–0.4	0.0	–0.7	–0.5	–0.8	–0.5	–0.2	–0.7
f_c (cloud fraction)	–0.5	0.0	1.2	0.9	0.2	0.9	–0.2	0.1
w_g (soil moisture)	–0.5	–0.7	0.9	0.6	0.4	0.6	0.0	0.8
$w_{g_{res}}$ (w_g residual)	0.0	–0.6	0.7	0.7	0.4	0.3	0.0	0.7
S_c, w_g	–0.9	–0.7	0.2	0.1	–0.5	0.2	–0.2	0.0

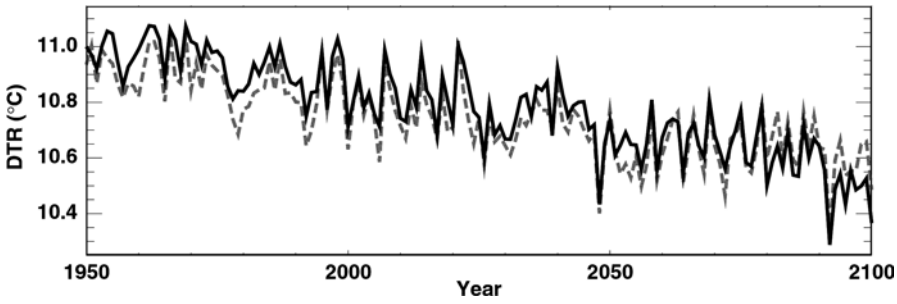

Fig. 5 Regression model estimate of annual mean variations in the DTR from CGCM1 GHG + A1 averaged over non-polar land areas. The regression time series, the *black solid line*, is estimated using downward solar radiation and soil moisture. The model DTR variations, the *grey dashed line*, are shown for comparison

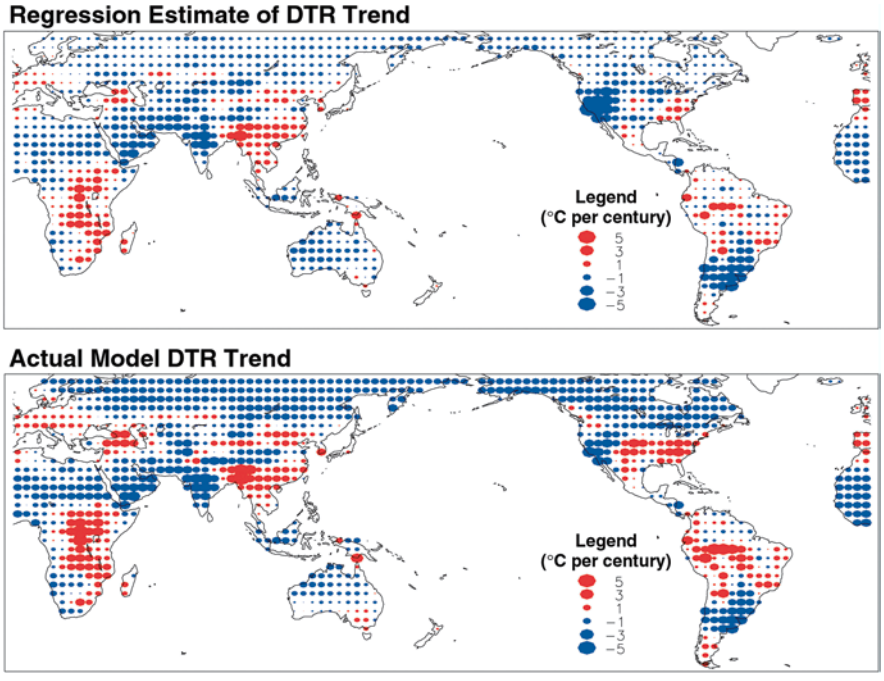

Fig. 6 Map of the 1950–2100 annual mean trends in the DTR in CGCM1 GHG + A1 estimated from the regression model using downward solar radiation and soil moisture. A map of the actual model DTR trends is shown for comparison

Thus the question arises as to the relative importance of both variables. To examine this we decompose S_c and w_g into

$$S_c = S_{c_{corr}} + S_{c_{res}}$$
$$w_g = w_{g_{corr}} + w_{g_{res}}$$

where $S_{c_{res}}$ ($w_{g_{res}}$) is the residual after the removal of the component $S_{c_{corr}}$ ($w_{g_{corr}}$) correlated with w_g (S_c).

The correlations of the DTR estimates of these residuals with the model DTR in CGCM1 GHG + A1 are listed in Table 5. The two residuals account for comparable portions of the variance of the DTR, with $S_{c_{res}}$ being slightly more important. The magnitudes of the DTR trend estimates based upon each of the residuals (Table 6) are also quite similar. The equal importance of solar radiation and soil moisture for the DTR trend found here differs from the predominance of solar radiation suggested by the analytic model. This could reflect the separation in Eq. (4) of soil moisture from the ground albedo and latent heat flux, both of which depend strongly upon it. However, in the model integrations changes in the latent heat flux are generally balanced by the sensible heat flux. Inherent in this point, of course, is the assumption that both heat fluxes exhibit similar diurnal cycles. Furthermore, when variations in the ground albedo and latent heat flux are included in Eq. (4), the estimates in fact generally worsen. A plausible explanation is the substitution of the 2 m air temperature T for T_g in Eq. (4), which systematically underestimates the diurnal amplitude of T_g (Peel 1974; Jin et al. 1997) and thus the magnitude of its effect on the DTR.

6 Middle latitude winter

The results of the previous two sections indicate that in most seasons and locations the DTR trends result primarily from combined changes in clouds and soil moisture. However, this relation does not hold for the middle latitude winters. This discrepancy is important, since the largest DTR decrease occurs at this time. We examine this case more closely in this section.

The daily average DTR as a function of the daily mean temperature is displayed in Fig. 7 for the DJF season in the northern middle latitudes. Daily values at each grid point over the 1961–1980 period from

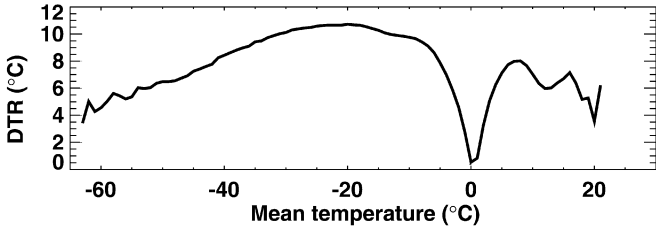

Fig. 7 The daily average DTR as a function of the daily mean temperature. 1961–1980 daily data for the DJF season, covering grid boxes in the northern middle latitudes, are used from CGCM1 GHG + A1

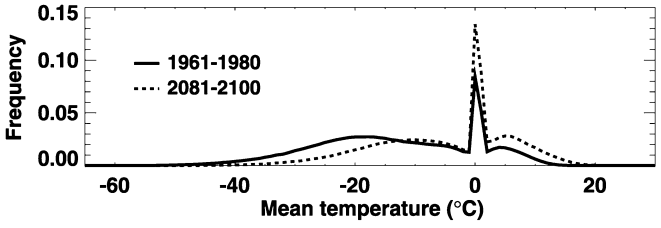

Fig. 8 The frequency of days and grid boxes with given mean temperatures during the DJF season in the northern middle latitudes. The frequencies for the 1961–1980 and 2081–2100 periods in CGCM1 GHG + A1 are shown

CGCM1 GHG + A1 are used. The most striking feature of this figure is the much lower DTR values that occur on days when the mean temperature is near 0 °C. As noted by Kharin and Zwiers (2000), this is an artifact of CGCM1's land surface model. (CGCM2 also uses this land surface scheme and thus is similarly impacted.) CGCM1 represents the land surface as a single layer. Due to energy balance constraints, the temperature near the surface does not drop substantially below the freezing point until all of the soil moisture in the layer freezes. Thus, on days with a mean temperature near 0 °C, the diurnal cycle of the energy flux into the ground is often insufficient to completely freeze of melt soil moisture, resulting in little change in the screen level temperature over the diurnal cycle.

During the 1961–1980 period, most winter days and grid boxes in the northern middle latitudes are below the freezing point, with the average being –11.8 °C (Fig. 8). However, these latitudes warm by 7.9 °C by the 2081–2100 period, resulting in a much higher frequency of days and grid boxes near 0 °C. This implies a higher frequency of days with a very small DTR. We can estimate the effect of this shift to more frequent days near the freezing point by integrating the product of the T_0 probability density function of 2081–2100 in Fig. 8 with the DTR-T_0 function from 1961–1981 in Fig. 7. The result is a 1.3 °C decrease in the DTR. The actual model decrease between these two time periods is 1.4 °C, so this shift to more frequent days and grid boxes near the freezing point accounts for most of the change.

During the southern middle latitude winter, this shift in mean temperature near 0 °C is also important. However, since most of the land here is near the low latitudes and the mean temperature is usually above freezing, this leads to an increase in the DTR which is moderated by the influence of clouds and soil moisture. Since the mean temperature seldom reaches the freezing point in the other seasons in either the northern or southern middle latitudes, the DTR is not susceptible to this effect, and so the trends arise primarily as a consequence of changes in clouds and soil moisture. The same applies to all seasons in the low latitudes.

7 Discussion and conclusions

Recent modelling studies support the theory that anthropogenic forcing of climate will induce a decrease in the DTR. However, the predicted magnitude of this trend is much smaller than observed. Here we have examined the trends in global warming integrations of a coupled GCM, and found decreases similar to those in previous studies. Trends tend to be largest in the middle latitudes, and possess distinct seasonal signatures, although these are different in either hemisphere.

Variations in the DTR are considerably more sensitive to changes in feebacks than in the direct forcings. In particular, projected decreases result from the combined effects of changes in clouds and in soil moisture, consistent with the findings of previous observational studies (Karl et al. 1993; Dai et al. 1997, 1999) and modelling studies (Stenchikov and Robock 1995; Dai et al. 2001). The main impact of clouds is to reduce the downward solar radiation during the day, and thus reduce T_{max}. Thus the reduction in solar radiation in the CGCM1 GHG + A1 integration arises either through an increase in the mean cloud albedo or through a shift in the diurnal cycle of cloud cover, since the average cloud cover changes little. The former alternative is supported by the increase in precipitation occurring in the intergration, since this implies thicker and more reflective clouds, and it is supported by observational studies (Dai et al. 1997). Notably, the scattering of sunlight by sulfate aerosols is found to have a negligible impact on the DTR, as found in other modelling studies (Mitchell et al. 1995; Reader and Boer 1998). It should be noted however that this coupled model lacks a representation of the indirect effect of aerosols; since this effect modifies the optical properties of clouds, it could have an important influence on the DTR trends.

The exceptions to the relation of the DTR to solar radiation and soil moisture occur during the winter seasons in the middle latitudes. The reflective and insulative properties of snow reduce the effect these variables would otherwise have. Nevertheless, the largest decrease in the DTR occurs at this time. There is a tendency in CGCM1 for the DTR to be very small when the mean temperature is near the freezing point. The DTR trends during the winter result from a shift to a higher or lower frequency of days near the freezing point, and thus with

very small DTR values. It should be noted that this effect is an artifact of land surface scheme in CGCM1 (and CGCM2) and so the affected trends cannot be considered realistic.

Analysis of the effects of soil moisture on the DTR trends indicate that its influence is comparable to that of clouds in the model integrations. Much of this effect arises through its control of the ground heat capacity, although the comparison of the analytic and regression models in Sect. 4 and 5 indicates that this can probably not fully account for the response. Other influences arise through control of the ground albedo and the latent heat flux. While both of these were represented in the analytical model, the representation of the latent heat flux assumed a similar diurnal cycle to the sensible heat flux, and the anti-correlation between the two heat fluxes resulted in a cancellation of their effects, consistent with the findings of observational studies (Dai et al. 1999). However, both variables are individually highly correlated with the DTR, and so relatively small deviations from this assumption may be important enough to give rise to the discepancy in the effect of soil moisture. While the use of a single layer model for the land surface scheme limits the applicability of using the coupled model output for predictive purposes, it does indicate the potential for an important influence of land surface processes on the DTR. For example, this implies that the physiological responses of vegetation to climate change, which are not represented in CGCM1, could be important in determining the tendency of the DTR, as proposed by Collatz et al. (2000). Also, although observational studies suggest that changes in land use are not a primary factor behind the observed DTR trend (Easterling et al. 1997; Gallo et al. 1999), the importance of soil moisture found here implies that this effect requires further observational and modelling study.

These results indicate that anthropogenic forcing could induce a decrease in the DTR, through changes in clouds and in land processes. Naturally, these results depend on the ability of the coupled model to represent these two components, whose behaviour under climate change is amongst the least understood of all processes. Consequently, much of the current activity in model development is concentrated on these two factors. The resulting improvements should soon permit a more confident determination of the behaviour of the DTR under anthropogenic forcing. At this stage, however, it is possible to identify these two factors as the primary influence on the DTR under climate change.

Acknowledgements The authors wish to thank George Boer, Slava Kharin, Daniel Robitaille, and the Canadian Centre for Climate Modelling and Analysis for supplying the data used in this analysis, as well as two anonymous reviewers for suggestions that improved the manuscript. Financial support for this research from the Climate Change Action Fund, the Meteorological Service of Canada/Canadian Institute for Climate Studies, the National Sciences and Engineering Research Council/Canadian Foundation of Atmospheric Studies CLIVAR project, and the National Sciences and Engineering Research Council is gratefully acknowledged.

References

Barry RG, Chorley RJ (1992) Atmosphere, weather and climate sixth edn, Routledge, New York, pp 392

Boer GJ, Flato GM, Ramsden D (2000a) A transient climate change simulation with greenhouse gas and aerosol forcing: projected climate to the twenty-first century. Clim Dyn 16: 427–450

Boer GJ, Flato GM, Reader MC, Ramsden D (2000b) A transient climate change simulation with greenhouse gas and aerosol forcing: experimental design and comparison with the instrumental record for the twentieth century. Clim Dyn 16: 405–425

Cao HX, Mitchell JFB, Lavery JR (1992) Simulated diurnal range and variability of surface temperature in a global climate model for present and doubled CO_2 climates. J Clim 5: 920–943

Collatz GJ, Bounoua L, Los SO, Randall DA, Fung IY, Sellers PJ (2000) A mechanism for the influence of vegetation on the response of the diurnal temperature range to changing climate. Geophys Res Lett 27: 3381–3384

Colman RA, Power SB, McAvaney BJ, Dahni RR (1995) A non-flux corrected transient CO_2 experiment using the BMRC coupled atmosphere/ocean GCM. Geophys Res Lett 22: 3047–3050

Dai A, Del Genio AD, Fung IY (1997) Clouds, precipitation and temperature range. Nature 386: 665–666

Dai A, Trenberth KE, Karl TR (1999) Effects of clouds, soil moisture, precipitation, and water vapor on diurnal temperature range. J Clim 12: 2451–2473

Dai A, Wigley TML, Boville BA, Kiehl JT, Buja LE (2001) Climate of the twentieth and twenty-first centuries simulated by the NCAR Climate System Model. J Clim 14: 485–519

Durre I, Wallace JM, Lettenmaier DP (2000) Dependence of extreme daily maximum temperatures on antecedent soil moisture in the contiguous United States during summer. J Clim 13: 2641–2651

Easterling DR, Horton B, Jones PD, Peterson TC, Karl TR, Parker DE, Salinger MJ, Razuvayev V, Plummer N, Jamason P, Folland CK (1997) Maximum and minimum temperature trends for the globe. Science 277: 364–367

Flato GM, Hibler III WD (1992) Modelling pack ice as a cavitating fluid. J Phys Oceanogr 22: 626–651

Flato GM, Boer GJ (2001) Warming asymmetry in climate change simulations. Geophys Res Lett 28: 195–198

Flato GM, Boer GJ, Lee WG, McFarlane NA, Ramsden D, Reader MC, Weaver AJ (2000) The Canadian Centre for Climate Modelling and Analysis global coupled model and its climate. Clim Dyn 16: 451–467

Gallo KP, Owen TW, Easterling DR, Jamason PF (1999) Temperature trends of the US historical climatology network based on satellite-designated land use/land cover. J Clim 12: 1344–1348

Gent PR, McWilliams JC (1990) Isopycnal mixing in ocean circulation models. J Phys Oceanogr 20: 150–155

Jin M, Dickinson RE (2002) New observational evidence for global warming from satellite. Geophys Res Lett 29(10): (39:1–4) 10.1029/2001GL013833

Jin M, Dickinson RE, Vogelmann AM (1977) A comparison of CCM2-BATS skin temperature and surface-air temperature with satellite and surface observations. J Clim 10: 1505–1524

Karl TR, Jones PD, Knight RW, Kukla G, Plummer N, Razuvayev V, Gallo KP, Lindseay J, Charlson RJ, Peterson TC (1993) Asymmetric trends of daily maximum and minimum temperature. Bull Am Meteorol Soc 74: 1007–1023

Kharin VV, Zwiers FW (2000) Changes in the extremes in an ensemble of transient climate simulations with a coupled atmosphere-ocean GCM. J Clim 13: 3760–3788

McFarlane NA, Boer GJ, Blanchet JP, Lazare M (1992) The Canadian Climate Centre second-generation general circulation model and its equilibrium climate. J Clim 5: 1013–1044

Mitchell JFB, Davis RA, Ingram WJ, Senior CA (1995) On surface temperature, greenhouse gases, and aerosols: models and observations. J Clim 8: 2364–2386

New M, Hulme M, Jones P (2000) Representing twentieth-century space-time climate variability. Part II: development of 1901–96 monthly grids of terrestrial surface climate. J Clim 13: 2217–2238

Peel RF (1974) Insolation and weathering: some measures of diurnal temperature changes in exposed rocks in the Tibesti region, central Sahara. Z Geomorph Supp 21: 19–28

Reader MC, Boer GJ (1998) The modification of greenhouse gas warming by the direct effect of sulphate aerosols. Clim Dyn 14: 593–607

Stenchikov GL, Robock A (1995) Diurnal asymmetry of climatic response to increased CO_2 and aerosols: forcings and feedbacks. J Geophys Res 100: 26,211–26,227

Stone DA, Weaver AJ (2002) Daily maximum and minimum temperature trends in a climate model. Geophys Res Lett 29(9): (70:1–4) 10.1029/2001GL014556